Assessment of Tropical Cyclone Risk in the Pacific Region

Technical Report

GEOSCIENCE AUSTRALIA

Craig Arthur, Martine Woolf

Australian Government
Geoscience Australia

Department of Resources, Energy and Tourism

Minister for Resources and Energy: The Hon Gary Gray AO MP
Secretary: Mr Blair Comley, PSM

Geoscience Australia
Chief Executive Officer: Dr Chris Pigram
This paper is published with the permission of the CEO, Geoscience Australia

Contents

Acknowledgements

Geoscience Australia acknowledges the contributions of the Department of Industry, Innovation, Climate Change, Science, Research and Tertiary Education (DIICCSRTE) for supporting this work as part of the Pacific-Australia Climate Change Science and Adaptation Planning Program. Data was provided by the International Best Track Archive for Climate Stewardship (IBTrACS), the Commonwealth Scientific and Industrial Research Organisation (CSIRO) Marine and Atmospheric Research Division, the World Climate Research Program's (WCRP) Coupled Model Intercomparison Project Phase 3 and 5 (CMIP3 and CMIP5), with thanks to the climate modelling groups (Table 12) for producing and making available their data.

Glossary

CMIP	Coupled Model Intercomparison Project. CMIP3 represents the third phase of the project, where the outputs were used in the Intergovernmental Panel on Climate Change's (IPCC) Fourth Assessment Report. CMIP5 represents the fifth phase, and those model outputs are to be used in the IPCC Fifth Assessment Report.
CSIRO	Commonwealth Scientific and Industrial Research Organisation
DIICCSRTE	Department of Innovation, Industry, Climate Change, Science, Research and Tertiary Education
Dynamical downscaling	The output from a GCM is used to drive a RCM, which is run at higher spatial resolution. The process allows smaller scale features of the climate to be better resolved, while retaining large-scale characteristics from the GCM.
GCM	A general circulation model (also commonly referred to as global climate model) is a mathematical model of the atmosphere (and ocean) used for weather and climate modelling applications
GHG	Green House Gas
IBTrACS	International Best Track Archive for Climate Stewardship. The official archiving and distribution resource for tropical cyclone best track data, endorsed by the World Meteorological Organisation.
ICCAI	International Climate Change Adaptation Initiative
PACCSAP	Pacific-Australia Climate Change Science and Adaptation Planning Program
PCRAFI	Pacific Catastrophe Risk Assessment and Financing Initiative
RCM	Regional climate model. Similar to a GCM, but restricted to a reduced domain.

RCP	Representative Concentration Pathways (van Vuuren et al., 2011). A set of four socio-economic and emission scenarios developed for the climate modelling community as a basis for long-term modelling experiments.
RSMC	(Tropical Cyclone) Regional Specialized Meteorological Centre. A centre responsible for detecting tropical cyclones, providing basic information about the systems present and forecast position, movement and intensity information on tropical cyclones within its designated area of responsibility.
SRES	Special Report on Emission Scenarios (Nakicenovic and Swart 2000). A set of scenarios that represent the range of driving forces and emissions that are used as a basis for long-term modelling experiments.
TCLV	Tropical Cyclone-Like Vortex. A feature in climate model output that has characteristics similar to observed TCs, such as a warm core and closed circulation.
WMO	World Meteorological Organisation

Introduction

The Assessment of Tropical Cyclone Risks in the Pacific Region project represents a collaboration between DIICCSRTE and Geoscience Australia with PCRAFI and AIR Worldwide. Building on the expertise of each organisation, the project will deliver an assessment of the financial risks to buildings, infrastructure and agriculture arising from tropical cyclones (TCs) under current and future climate regimes. This extends previous risk assessments undertaken by incorporating the influence of climate change on the hazard (TCs) into the assessment process.

Operating as part of the Pacific-Australia Climate Change Science and Adaptation Planning Program (PACCSAP), the project aims to improve the understanding of financial risks posed by tropical cyclones to key assets in Partner Countries (Cook Islands, Fiji, Kiribati, Federated States of Micronesia, the Republic of the Marshall Islands, Nauru, Niue, Palau, Papua New Guinea, Samoa, Solomon Islands, Timor Leste, Tonga, Tuvalu and Vanuatu) in the Pacific region under future climate scenarios. The objective of the project is for Partner Country governments to be able to better integrate climate risk considerations into infrastructure planning and development and ex-ante disaster planning.

Knowledge of the current level of risk - and the way that risk will change into the future - will aid decision makers in prioritising adaptation options around issues such as land-use zoning, crop choice and urban infrastructure planning. This information is also valuable for highlighting the risks of inaction around climate change in negotiations for mitigation actions at the international level.

Geoscience Australia's role is to evaluate datasets derived from general circulation models (GCMs) to inform tropical cyclone risk assessments performed by AIR Worldwide. This document describes the data and methods used for the analysis, and presents a summary of this data analysis.

The output of this study is a set of *peril matrices*, which detail the relative change in parameters describing TC behaviour: e.g. annual mean frequency, mean maximum intensity and mean latitude of genesis. The relative changes are evaluated as the fractional change between TC behavior in current climate GCM simulations and future climate GCM simulations.

In parallel with this data analysis project, Geoscience Australia is engaging with Pacific Island representatives to evaluate appropriate delivery mechanisms for this risk information and complementary TC hazard information. A key goal to achieving the objectives of the PCRAFI project is to ensure stakeholders have ready access to this information, and can also integrate the information with their own existing information and datasets relating to risk. Geoscience Australia will also be scoping a training program that intends to meet the goal of providing training on developing and utilising risk information from local data on the exposure and vulnerability of assets.

Study area

The study area covers the South Pacific Ocean, Western North Pacific Ocean and the far eastern parts of the Southern Indian Ocean (Figure 1). Covered by the study area are the 15 PACCSAP Partner countries: Cook Islands, Fiji, Kiribati, Federated States of Micronesia, the Republic of the Marshall Islands, Nauru, Niue, Palau, Papua New Guinea, Samoa, Solomon Islands, Timor Leste, Tonga, Tuvalu and Vanuatu. The countries exposed to the greatest threat of TCs are those between 10 and 30 degrees from the equator. Nauru, Kiribati and Tuvalu have a comparatively low threat from TCs, due to their proximity to the equator. This does not mean that the threat of TCs can be ignored, as historically intense TCs have passed within a few degrees of the equator (e.g. Typhoon *Kate* (1970) and Typhoon *Bopha* (2012); also see Brunt 1969).

In both hemispheres, the domain spans from 120°E to 120°W. The northern hemisphere domain extends from the equator to 25°N, while the southern hemisphere domain extends to 35°S. These domains capture the track of all historical TCs that have impacted the Partner countries.

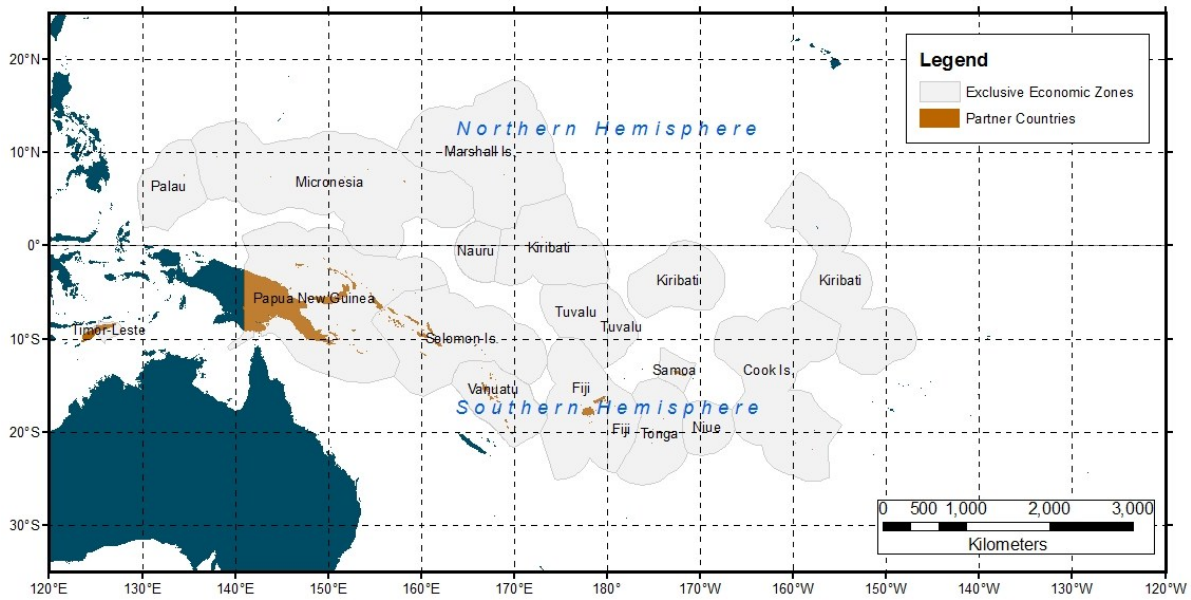

Figure 1: PACCSAP Partner Countries (and their Exclusive Economic Zone) and domain extent for the northern and southern hemispheres.

Source data

To understand the changes in TCs under future climate conditions, information not only on the future state of TC activity, but information on the current state is required. Information can be extracted from the historical record of TC activity through exploration of historical databases that contain intensity and position information on past events. To look forward we must rely on simulations of future climate, and the features within those simulations that resemble TCs.

In this study, we assume that the projected relative changes (differences between current climate simulations and projected climate simulations) are a good indicator of likely changes in TC behaviour, and apply these relative changes in behaviour to the historical behaviour to describe future behaviour. For example, if the future climate simulation indicates a 10% increase in TC frequency relative to the current climate simulation, the projections here apply a 10% increase to the historical (observed) TC frequency.

Tropical Cyclone-Like Vortices

Tropical Cyclone-Like Vortices (TCLVs) are features in GCMs that have characteristics similar to observed TCs. Based on objective criteria, vortices in the GCM output can be identified and tracked to produce a database of events that have characteristics similar to observed TCs. The identification and tracking of TCLVs was performed by CSIRO Marine and Atmospheric Research as part of the PACCSAP Science Program and the outputs provided to Geoscience Australia.

The identification and tracking algorithm is based on the works of Nguyen and Walsh (2001), Walsh and Syktus (2003) and Abbs et al., (2006). The procedure uses several criteria for identifying TCs:

(1) vorticity more negative than -10^{-5} s^{-1} (as cyclonic vorticity is negative in the Southern Hemisphere);

(2) closed pressure minimum, taken to be the centre of the storm, within 250 km from a point satisfying the first criterion. The 250 km distance was empirically chosen to give a good geographic association between vorticity maxima and pressure minima;

(3) total tropospheric temperature anomalies at 750, 500 and 300 hPa (i.e. the variation of temperature at the centre of the storm from the mean environmental temperature) must be greater than zero, signifying that the storm has a warm core;

(4) mean wind speed in the area 500 km × 500 km around the centre of the storm at 850 hPa must be higher than that at 300 hPa;

(5) temperature anomaly at 300 hPa must be at least 0.6°K;

(6) outer core wind strength, which is defined as the mean tangential wind speed between a 1° and 2.5° radius of latitude from the storm centre, must be above 0 m s^{-1};

(7) maximum 10 m wind speed in the storm at any one time must be at least 12.5 m s^{-1}; and

(8) rotation, as defined by the wind direction around the storm centre, must be present.

Once a TC is detected, criteria 3, 4 and 5 are relaxed. The storm track is followed until one of criteria 1, 2, 6 or 7 are no longer satisfied (the wind speed dropped, the vorticity weakened or the closed low pressure centre disintegrated). Further details of the vortex identification and tracking technique used for this project are described in Abbs (2012).

Two sources of TCLVs were used in this study. The first were a set of TCLVs extracted from dynamically-downscaled simulations based on CMIP3 GCM simulations. The downscaling process was performed using the CSIRO Conformal-Cubic Atmospheric Model (CCAM) of McGregor and Dix (McGregor et al., 2008) to 65 km horizontal grid spacing, forced by bias-corrected sea surface temperature fields (BoM and CSIRO, 2011). Six models were downscaled in this manner (CSIRO Mk 3.5, ECHAM5, GFDL CM2.0, GFDL CM2.1, UK HadCM3 and MIROC 3.2 medres)[1]. The resulting gridded fields were used for the identification and tracking process to extract TCLV events.

The second set of TCLVs was direct-detections from the CMIP5 collection of GCMs. In this case, the raw GCM data was used for identifying and tracking the TCLVs, due to the improved horizontal resolution of the newer generation of models. Five models were available through this technique (ACCESS 1.0, Can ESM2, CSIRO Mk3.6.0, IPSL CM5A LR and Nor ESM1 M).

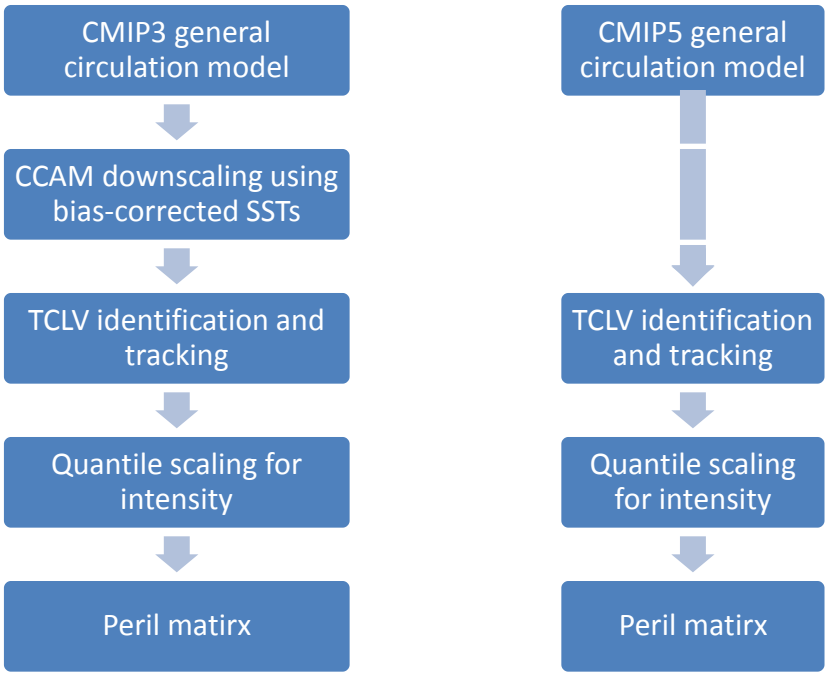

Figure 2: Conceptual flow of information for generating TCLV datasets and resulting peril matrices.

The dynamical downscaling applied to the CMIP3 models introduces an additional source of influence on the derived results. The sea-surface temperature bias correction method used to drive the CCAM simulations produces forcing conditions that are highly correlated across the suite of models. While

[1] See the Appendix for a list of model names and corresponding groups.

this improves the model performance for current climate simulations (Katzfey et al., 2009), basic large-scale features of the GCMs may be lost through this process. As such, it is to be expected that results from this process will be very similar. Figure 2 presents the conceptual flow of information from the GCMs to the peril matrices for the CMIP3 and CMIP5 GCMs.

It is also important to note that the emission scenarios underpinning the CMIP3 and CMIP5 simulations are not directly comparable. That is, the SRES A2 scenario indicates a different societal and technology pathway, and hence different GHG emission pathway, than the RCP 8.5 scenario (van Vuuren et al., 2011). This results in different climate projections between the two generations of models.

Historical tropical cyclone track data

For this project, Geoscience Australia used the International Best-Track Archive for Climate Stewardship[2] (IBTrACS) global tropical cyclone database to represent historical TC activity (Knapp et al. 2010). The IBTrACS database collates information on TC tracks and intensity from reporting agencies around the globe and provides a single authoritative database that can be used for climate analysis. By drawing data from World Meteorological Organisation (WMO) Regional Specialized Meteorological Centers (RSMCs) and other international agencies, the IBTrACS dataset contains the most complete global set of historical TCs available. For this study, we use the IBTrACS (version 3, revision 4) WMO dataset, which includes only those records provided by WMO RSMCs. Figure 3 shows the tracks contained within the IBTrACS dataset for the period 1981-2011.

Note that in the northern hemisphere, AIR Worldwide's catastrophe model is based on the Japanese Meteorological Agency (JMA) best track record, which excludes all TC events forming east of 180°E. This produces differences in the mean annual frequency of storms in the region of interest. As the JMA best track dataset is the primary dataset in IBTrACS west of 180°E, the remaining parameters are only moderately affected.

[2] IBTrACS: http://www.ncdc.noaa.gov/oa/ibtracs/

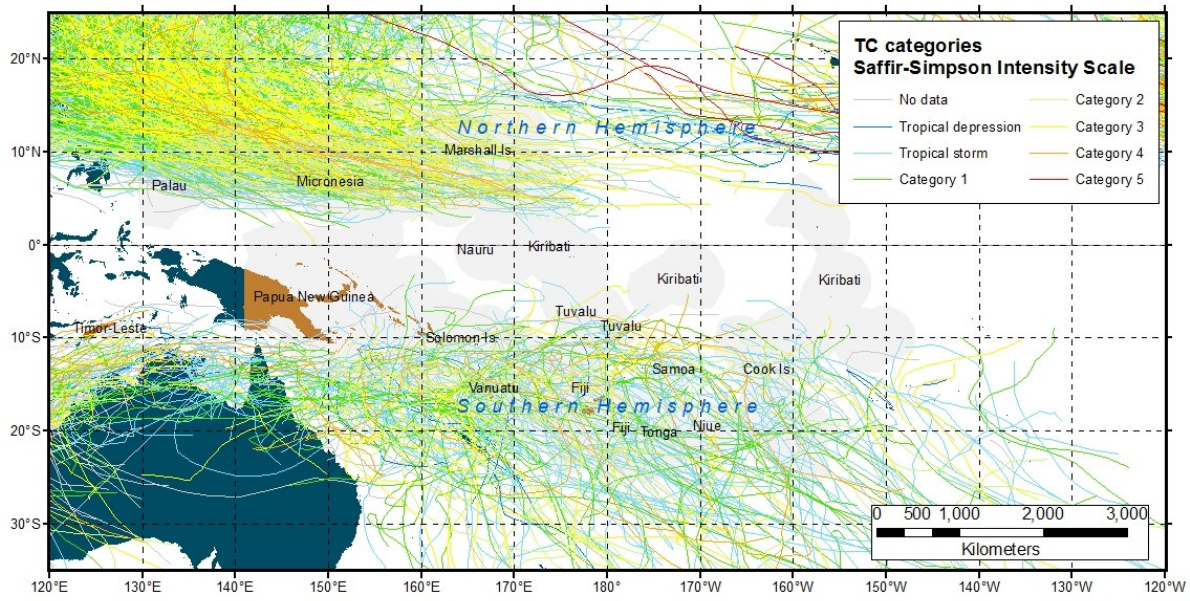

Figure 3: Historical TC's in the PCRAFI region (1981-2011). Colours of tracks indicate maximum lifetime intensity of the storm. Exclusive economic zones of PCRAFI countries are indicated in grey.

Methods

Parameters

Following is a list of all parameters evaluated for this project. Each parameter is evaluated within a domain (northern or southern hemisphere) and for a given time period (observed, current climate and future climate). These parameters are used by AIR Worldwide to control the selective sampling of a catalog of synthetic TC events as part of the loss modelling process.

- Mean annual frequency (TCs/year);
- Mean latitude of TC formation (degrees N/S);
- Mean longitude of TC formation (degrees E);
- Mean latitude of maximum sustained winds (degrees N/S);
- Mean latitude of minimum central pressure (degrees N/S);
- Mean maximum sustained wind speed (m/s); and
- Mean minimum central pressure (hPa).

Additionally, we calculate the relative distribution of TC intensity based on seven classes based on the Saffir-Simpson Hurricane Intensity Scale. See subsequent sections for more details.

Central pressure deficit scaling

Due to the low horizontal resolution of GCMs, it is not possible for these models to accurately represent the fine-scale dynamical processes that control TC intensity. As such, the TCLV intensity distribution based on direct-detection methods is much lower than the observed record. To overcome this short-coming, we applied a quantile scaling process to the central pressure deficits (ambient sea level pressure minus central pressure) of the TCLVs. This allows us to bias correct the TCLV central pressure deficits to better match the observational data. Similar approaches have been applied to rainfall outputs from GCMs with reasonable success (e.g. Hemer et al., 2012).

We scaled the central pressure deficits using a parametric function - a combination of a power function and inverse tangent, where the power (β) is less than 1:

$$\Delta p_{scaled} = \frac{\alpha}{\pi} \Delta p_{TCLV}^{\beta} \tan^{-1}\left(\left[\frac{\Delta p_{TCLV}}{\chi}\right]^2\right) \qquad \textit{Eq 1}$$

A number of forms of the scaling function were tested, but were rejected due to the bias introduced at both very large deficits (i.e. intense storms) and small deficits. The large number of points at lower deficits dominated the input values, so only pressure deficits above the 50th percentile were used for

the fitting process. This weighs the scaling in favour of intense events – those events that cause the greatest damage. Further, a parametric function was chosen so that it is possible to extrapolate beyond the range of input Δp_{TCLV} values. The fitting process outlined below is based on current climate TCLV data, but is applied to projected TCLV data, where it is possible that the range of Δp_{TCLV} values is greater than in the current climate.

Quantiles for both the historical and current climate TCLV (1981-2000 period) datasets were calculated and the above function fitted using an unconstrained nonlinear minimisation of the sum of squared residuals, with respect to the parameters α, β and χ. Once fitted, the function is applied to both the current and projected climate TCLV datasets. The process is outlined below:

1. Sample *n* random values of Δp_{hist} (historical pressure deficit), where *n* is the number of Δp_{TCLV} records for 1981-2000 above the 50th percentile and within the domain of the analysis;
2. Repeat Step 1 1000 times and append to the previous values. Append the Δp_{TCLV} values to the vector of Δp_{TCLV} values as well. This produces two vectors of length *n*1000* containing randomly arranged pairs of historical and simulated Δp;
3. Calculate percentiles of each vector;
4. Run the fitting process on the vector of percentiles.

The scaling was performed independently for each hemisphere. That is, TCLVs in the southern hemisphere are scaled using only data (historical and TCLV) from the southern hemisphere. This improves the quality of the fit, especially in the southern hemisphere where there are fewer historical events on which to base the scaling compared to the northern hemisphere. Figure 4 and Figure 5 present the scaled central pressure deficits for the northern and southern hemisphere TCLV datasets respectively.

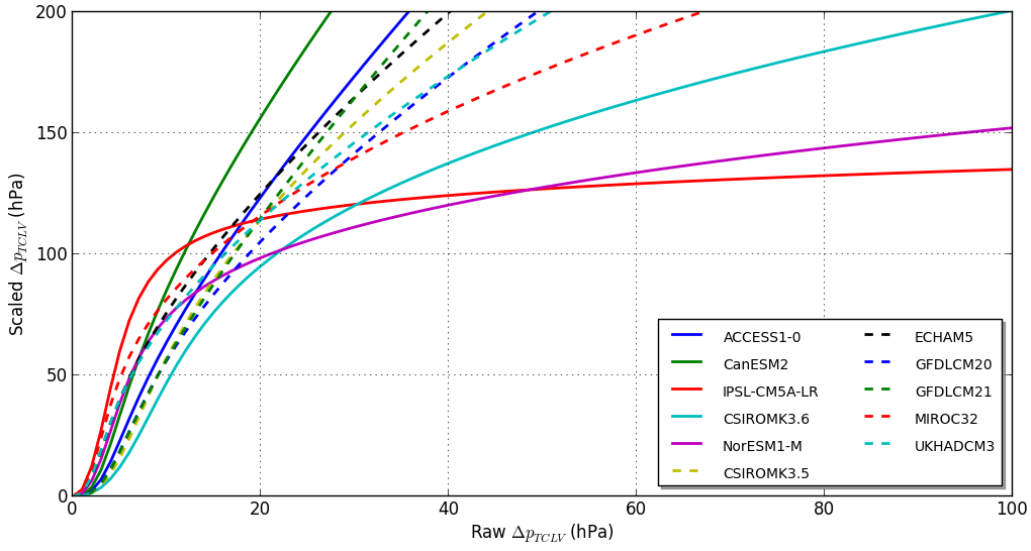

Figure 4: Scaling of central pressure deficit for the northern hemisphere. All CMIP3 models are indicated with dashed lines.

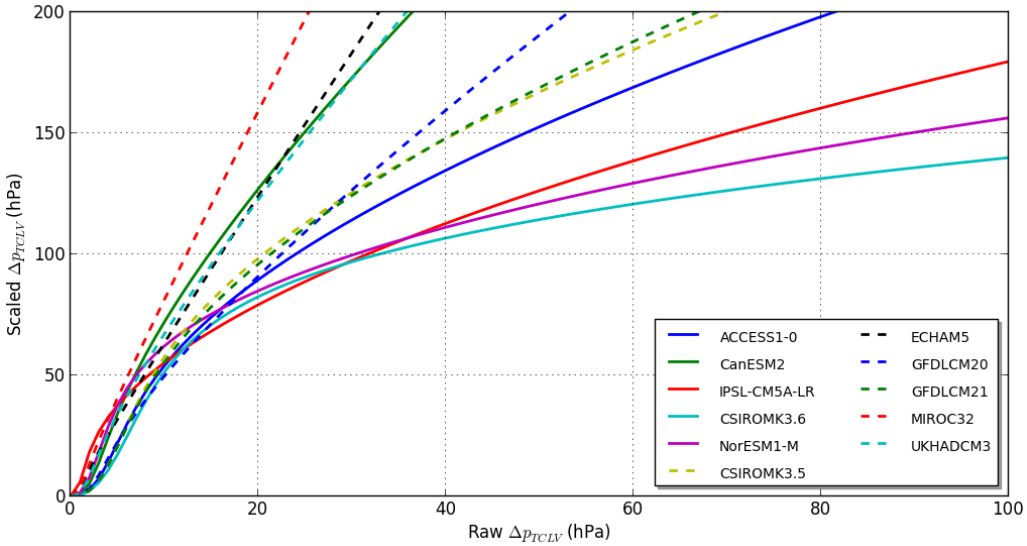

Figure 5: As for Figure 4, but for the southern hemisphere.

Figure 6 compares the quantiles for central pressure deficit for the historic and scaled current climate TCLV datasets for southern hemisphere data. Note only one model (IPSL CM5A) produces distributions that are statistically indistinguishable at the 5% level through the scaling process. In part, this result is due to using only quantiles above the 50th percentile for the scaling process. Therefore, the quality of fit at lower quantiles is reduced and the overall difference in distributions is dominated by the differences at these lower quantiles.

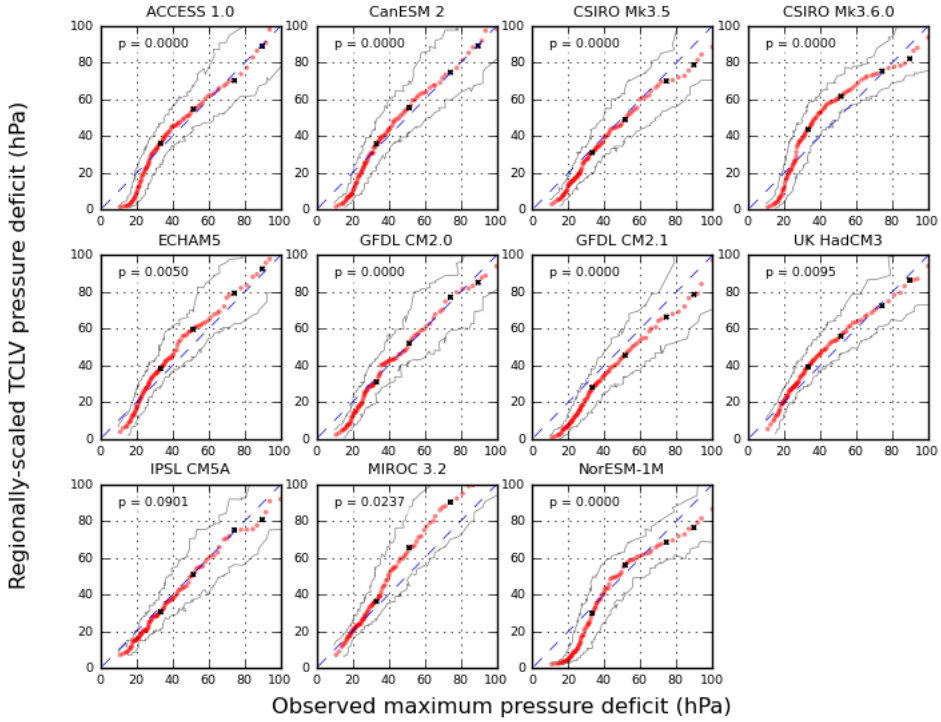

Figure 6: Quantile-quantile plot of central pressure deficits for observed TCs (horizontal axis) and scaled current climate TCLV dataset (vertical axis). Black points indicate 50th, 75th, 90th and 95th percentile values. Thin grey lines indicate 95th percentile. P-value is based on a Kolmogorov-Smirnov two-sample test for similar distributions.

Wind-pressure relations

To assign each TC event into a category for evaluation of changes in intensity as a function of wind speed, a wind-pressure relation was utilised to convert the central pressure deficits to a maximum sustained wind speed. There are a large number of wind-pressure relations available in the literature, and historically a range of relations have been used operationally (Harper, 2002). In the absence of coincident, independent observations of central pressure deficit and maximum wind speed, a statistical model is used.

For this analysis, the wind-pressure relation described in Holland (2008) as selected. This provided a 1-minute-mean sustained wind speed, which was then converted to a 10-minute mean wind speed using the recommendations contained in WMO TD-1555 (Harper et al., 2010), assuming “at-sea” surface conditions. The maximum wind speed derived through this process is referred to as the scaled maximum wind speed.

The quantile scaling process described previously results in a nearly-linear translation of the maximum wind speed. The TCLV data provides the raw model (or unscaled) maximum wind speed, as it is one of the objective criteria for identifying and tracking TCLVs. Figure 7 shows the relation between the scaled and unscaled maximum wind speeds is nearly linear, with nearly 98% of variance explained by a linear fit for the majority of models. Most wind-pressure relations can be described by a power-law relation, with a power less than one (Harper et al., 2002). The nearly-linear transformation in wind speed provides additional confidence that our choice of a power law scaling function for central pressure deficit is justified.

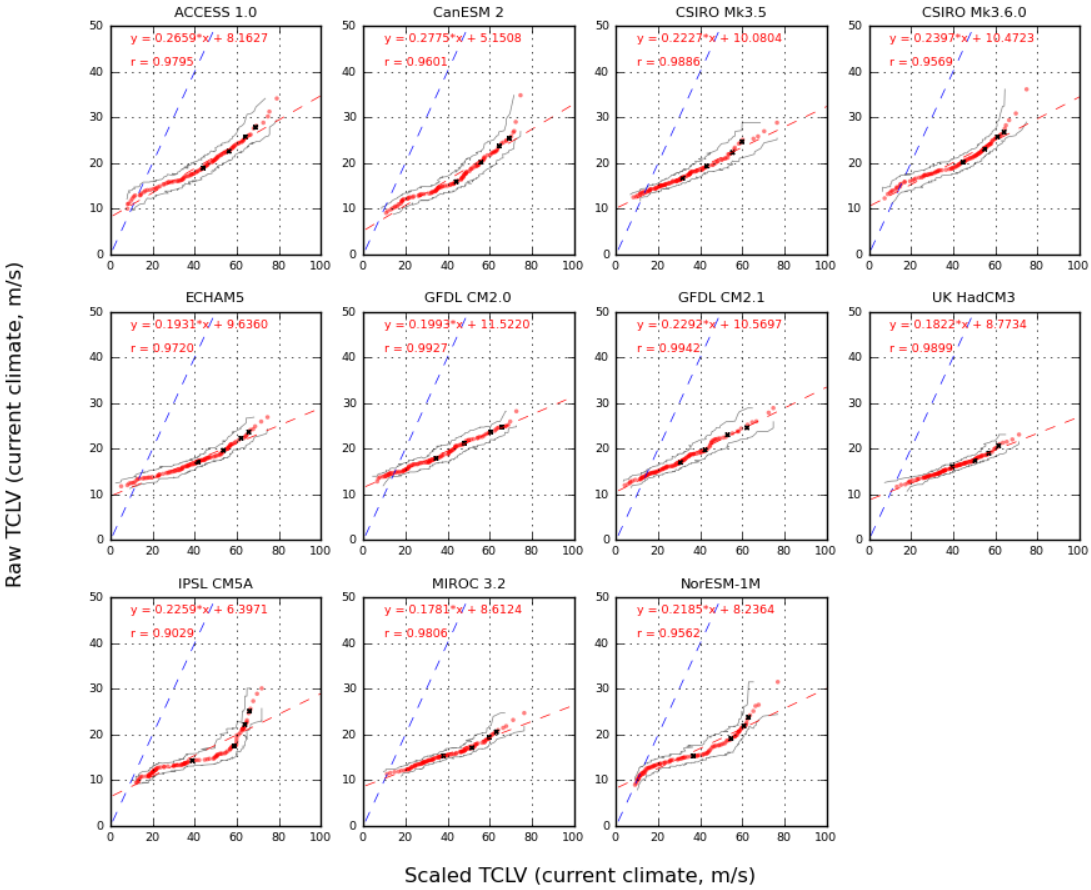

Figure 7: Quantile-quantile plot of scaled TCLV maximum wind speed (horizontal axis) and raw TCLV maximum wind speed (vertical axis). Black markers indicate the 50th, 75th, 90th and 95th percentile values. Grey lines indicate the 95th percentile range for each quantile. Blue dashed line has slope=1. Red dashed line represents linear fit to the data points, with the equation and correlation coefficient given in the top left corner of each panel.

Categorisation

TCs are categorised by the lifetime minimum central pressure into one of 7 classes, based on the Saffir-Simpson Hurricane Intensity Scale. We evaluate the distribution of TCs in each class and calculate changes in that distribution at 2050 and 2090. Also calculated is the baseline distribution of TC categories, using the historical track data.

Table 1: Classification of TCs based on maximum sustained winds and minimum central pressure, using the Saffir-Simpson Hurricane Intensity Scale.

Classification	1-minute sustained wind speed (m/s)	Minimum central pressure (hPa)
Tropical depression (TD)	< 17 m/s	>= 1005
Tropical Storm (TS)	17 – 32 m/s	1005 – 995
Category 1 (TC1)	32 – 42 m/s	995 – 980
Category 2 (TC2)	42 – 49 m/s	980 – 965
Category 3 (TC3)	50 – 58 m/s	965 – 945
Category 4 (TC4)	58 – 70 m/s	945 – 920
Category 5 (TC5)	> 70 m/s	< 920

Annual frequency calibration

Because of the different parameterisations, resolutions and forcing data used in the GCMs, each realisation produces a different number of events. In addition, the 20-year period of simulations used in this study may not be truly representative of the model 'climatology' of TC activity. This is due to interannual to interdecadal variability implicit in the GCMs, of which a 20-year period may provide only one snapshot.

The historical baseline is calculated from the IBTrACS (version 3, revision 4) WMO dataset for 1981 to 2011 inclusive. In some parts of the Pacific, TC activity is modulated by interannual and interdecadal oscillations (e.g. ENSO, PDO). This can mean the 31-year record used for the historical baseline may not be truly representative of long-term mean TC activity in the Pacific. For example, varying the baseline between 20 and 60 years results in the mean annual frequency varying by over 1 TC/year in both the northern and southern hemispheres (Table 2).

Note that the AIR Worldwide Catalog derives its statistics from the Japanese Meteorological Agency TC Best Track dataset in the Northern Hemisphere, which only covers TCs that form west of 180°E. This results in significant differences in mean annual frequency from those presented here.

Table 2: Annual mean frequency of TCs passing through each domain for different time spans. For all values, the end year is 2011. Based on IBTrACS v03r04 WMO dataset.

Start year	Northern hemisphere TC frequency	Southern hemisphere TC frequency
1951	32.6	12.8
1961	34.0	13.6
1971	34.4	14.4
1981	34.9	14.1
1991	34.0	13.2

For the peril matrices, the mean annual frequency of the current climate simulation is fixed for each GCM to match the historical baseline frequency for that domain. The relative change in mean annual frequency is calculated (fractional change between current and future climate simulations) and applied to the baseline to provide a projection of mean annual frequency at the future time period.

Significance testing

Changes in the mean value of a parameter were tested for significance using a Student's T-test for independent samples assuming unequal variances. Changes are considered significant when the *p*-value is less than 0.05.

Changes in distributions of a parameter were tested for significance using a Kolmogorov-Smirnov two-sample test. Again, changes are considered significant when the *p*-value is less than 0.05.

For ensemble change values, those values where the majority of members have the same sign, and are in the same direction as the mean, are considered to represent robust changes. This is not a statistical measure of significant change, but as a minimum provides guidance on whether a given outcome is more likely than not. As an indicator, for a 6 member ensemble, there is only a 10% chance of meeting this criterion through a random process, assuming the outcomes of that process are normally distributed.

Evaluating mid-century changes

To evaluate the changes in parameters at a mid-century timeframe, we linearly interpolate between the current climate and end-century values for each parameter. Researchers regularly estimate changes in climate-related parameters on the basis of a change proportional to the change in global mean temperature. For the CMIP5 models, RCP 8.5 shows an approximately linear increase in global mean temperature over the 21st century (Figure 8). For the CMIP3 models, the SRES A2 emission scenario displays a slightly exponential increase in global mean temperature through the 21st century (Figure 9). This may result in a slight over-estimation of the changes at the mid-century timeframe; however this difference is assumed to be statistically insignificant for the parameters being examined.

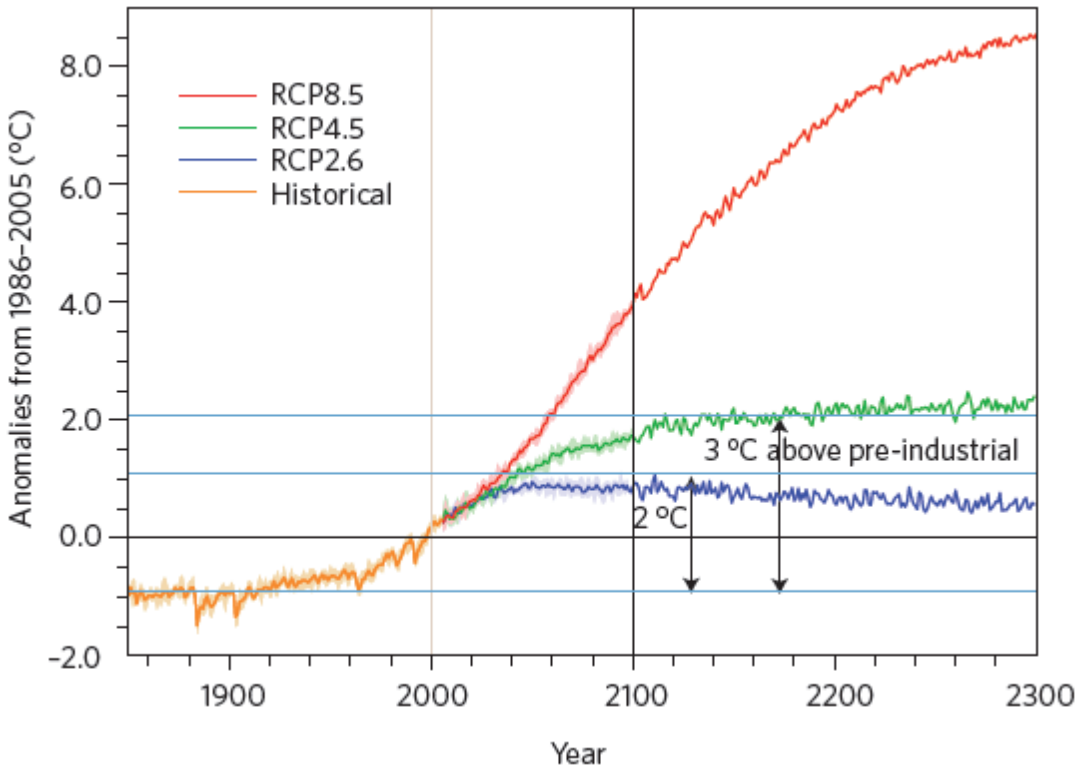

Figure 8: Time series of globally averaged surface air temperature anomalies from CCSM4, one of the CMIP5 models (using 1986–2005 as base period), for 1850 to 2005 (orange), and three RCP scenarios (RCP2.6, blue; RCP4.5, green; RCP8.5, red). Ensemble averages are solid lines (five-member ensembles to 2100, single members after 2100). Shading before 2100 is ±one standard deviation of the ensemble member values. Temperature changes of 2 °C and 3 °C compared with pre-industrial values are indicated with horizontal blue lines. From Meehl et al., 2012.

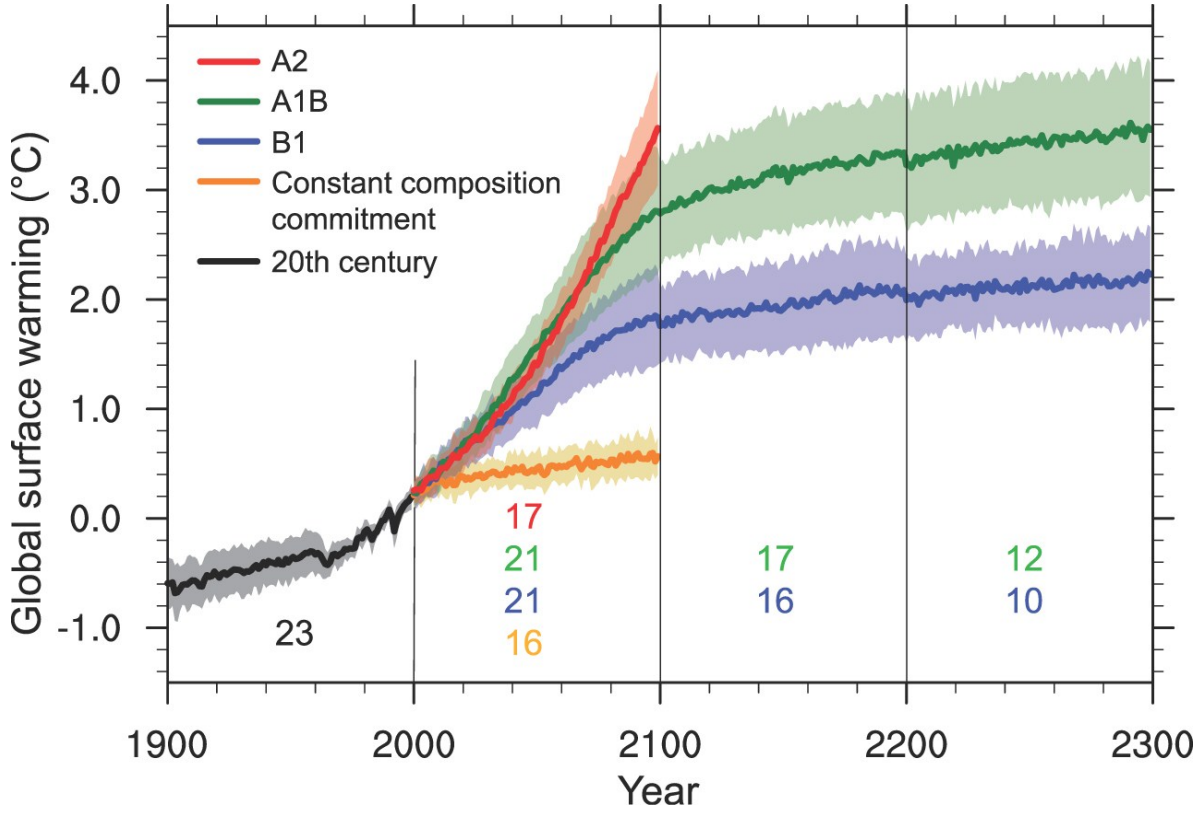

Figure 9: Multi-model means of surface warming (relative to 1980–1999) for the scenarios A2, A1B and B1, shown as continuations of the 20th-century CMIP3 simulation. Values beyond 2100 are for the stabilisation scenarios (see Section 10.7). Linear trends from the corresponding control runs have been removed from these time series. Lines show the multi-model means, shading denotes the ±1 standard deviation range of individual model annual means. Discontinuities between different periods have no physical meaning and are caused by the fact that the number of models that have run a given scenario is different for each period and scenario, as indicated by the coloured numbers given for each period and scenario at the bottom of the panel. For the same reason, uncertainty across scenarios should not be interpreted from this figure (from Meehl et al., 2007).

Results

Following are a series of tables detailing the changes in key parameters for the different time periods examined. Results are presented for 11 models – 5 CMIP5 models and 6 CMIP3 models. Full peril matrices have been passed to AIR Worldwide to generate climate-conditioned stochastic catalogs for evaluating TC-related losses.

In all cases, significant changes in the means (at the 5% level) are indicated by bold text.

Table 3: Mean annual frequency of tropical cyclones as simulated by TCLVs. Relative changes in TC frequency (percent change) are indicated in parentheses. 2081-2100 values in bold indicate a change that is significant at the 5% level. The historical baseline used is TC activity 1981-2011.

		Northern Hemisphere				Southern Hemisphere			
	Model	Historical baseline	1981-2000	2050	2081-2100	Historical baseline	1981-2000	2050	2081-2100
CMIP5	**ACCESS 1.0**	24.7	9.6	13.1	**15.4 (61.3%)**	13.2	13.6	12.2	11.3 (-17.0%)
CMIP5	**CanESM2**	24.7	19.8	20.5	21.0 (6.3%)	13.2	13.6	15.1	16.1 (18.8%)
CMIP5	**CSIRO Mk3.6.0**	24.7	25.1	24.4	23.9 (-5.0%)	13.2	14.4	12.3	**10.9 (-24.4%)**
CMIP5	**IPSL CM5A-LR**	24.7	12.4	15.7	**17.9 (43.8%)**	13.2	3.5	5.5	6.9 (100%)
CMIP5	**Nor ESM1**	24.7	13.7	12.3	11.4 (-16.5%)	13.2	13.2	12.1	11.3 (-14.4%)
CMIP3	**CSIRO Mk3.5**	24.7	15.1	12.5	**10.7 (-29.5%)**	13.2	8.9	6.0	**4.1 (-54.5%)**
CMIP3	**ECHAM5**	24.7	19.9	16.0	**13.4 (-32.7%)**	13.2	13.0	7.7	**4.1 (-68.5%)**
CMIP3	**GFDL CM2.0**	24.7	14.7	15.2	15.6 (6.5%)	13.2	9.3	5.5	**3.0 (-67.0%)**
CMIP3	**GFDL CM2.1**	24.7	17.3	13.9	**11.7 (-32.1%)**	13.2	9.9	6.1	**3.5 (-64.1%)**
CMIP3	**HadCM3**	24.7	21.0	21.1	21.2 (1.0%)	13.2	9.8	6.4	**4.1 (-57.9%)**
CMIP3	**MIROC 3.2**	24.7	14.7	13.4	12.5 (-15%)	13.2	7.0	3.8	**1.6 (-78.0%)**

Table 4: As for Table 3, but for mean latitude of genesis.

		Northern Hemisphere				Southern Hemisphere			
	Model	Historical baseline	1981-2000	2050	2081-2100	Historical baseline	1981-2000	2050	2081-2100
CMIP5	**ACCESS 1.0**	13.5	14.3	13.2	**12.5 (-12.2%)**	-14.3	-13.3	-12.5	**-11.9 (10.0%)**
CMIP5	**CanESM2**	13.5	15.0	14.7	14.5 (-3.2%)	-14.3	-13.3	-13.7	-14.0 (-5.6%)
CMIP5	**CSIRO Mk3.6.0**	13.5	14.6	14.3	14.2 (-2.6%)	-14.3	-14.3	-13.1	**-12.2 (15.0%)**
CMIP5	**IPSL CM5A-LR**	13.5	15.4	14.9	**14.6 (-5.5%)**	-14.3	-15.3	-15.5	-15.7 (-3.2%)
CMIP5	**Nor ESM1**	13.5	10.8	10.9	11.0 (2.5%)	-14.3	-12.6	-12.4	-12.2 (-3.2%)
CMIP3	**CSIRO Mk3.5**	13.5	16.2	15.6	**15.1 (-7.0%)**	-14.3	-19.3	-18.0	-17.1 (11.3%)
CMIP3	**ECHAM5**	13.5	15.0	15.0	15.0 (0.2%)	-14.3	-19.2	-20.8	**-21.8 (-13.4%)**
CMIP3	**GFDL CM2.0**	13.5	16.5	17.3	**17.9 (8.9%)**	-14.3	-22.1	-22.7	-23.1 (-4.8%)
CMIP3	**GFDL CM2.1**	13.5	16.4	16.5	16.6 (1.7%)	-14.3	-20.8	-23.1	**-24.6 (-18.5%)**
CMIP3	**HadCM3**	13.5	15.2	15.5	15.7 (3.3%)	-14.3	-14.1	-15.6	**-16.6 (-18.0%)**
CMIP3	**MIROC 3.2**	13.5	15.5	15.4	15.3 (-1.3%)	-14.3	-15.2	-17.1	**-18.3 (-20.2%)**

Table 5: As for Table 3, but for mean latitude of peak intensity (maximum sustained winds).

		Northern Hemisphere				Southern Hemisphere			
	Model	Historical baseline	1981-2000	2050	2081-2100	Historical baseline	1981-2000	2050	2081-2100
CMIP5	**ACCESS 1.0**	23.0	20.5	18.8	**17.7 (-13.5%)**	-20.2	-17.9	-17.2	-16.8 (6.7%)
CMIP5	**CanESM2**	23.0	17.2	17.3	17.4 (1.0%)	-20.2	-16.2	-17.3	**-18.1 (-11.8%)**
CMIP5	**CSIRO Mk3.6.0**	23.0	21.0	21.1	21.2 (1.1%)	-20.2	-21.0	-19.3	**-18.2 (13.1%)**
CMIP5	**IPSL CM5A-LR**	23.0	19.2	19.8	20.2 (5.3%)	-20.2	-22.2	-24.5	**-26.0 (-17.0%)**
CMIP5	**Nor ESM1**	23.0	14.7	14.4	14.2 (-3.5%)	-20.2	-16.0	-15.9	-15.9 (0.3%)
CMIP3	**CSIRO Mk3.5**	23.0	21.0	20.5	20.2 (-3.7%)	-20.2	-19.1	-19.1	-19.1 (0.3%)
CMIP3	**ECHAM5**	23.0	20.0	20.2	20.3 (1.4%)	-20.2	-19.2	-20.0	-20.4 (-6.3%)
CMIP3	**GFDL CM2.0**	23.0	20.8	21.8	**22.5 (8.2%)**	-20.2	-21.0	-21.3	-21.5 (-2.7%)
CMIP3	**GFDL CM2.1**	23.0	20.5	20.7	20.9 (2.0%)	-20.2	-18.5	-20.9	**-22.6 (-21.7%)**
CMIP3	**HadCM3**	23.0	19.9	20.1	20.3 (1.9%)	-20.2	-18.5	-20.2	**-21.3 (-14.8%)**
CMIP3	**MIROC 3.2**	23.0	20.5	19.9	**19.5 (-5.0%)**	-20.2	-19.0	-20.7	**-21.8 (-14.7%)**

Table 6: As for Table 3, but for mean latitude of peak intensity (minimum central pressure).

		Northern Hemisphere				Southern Hemisphere			
	Model	Historical baseline	1981-2000	2050	2081-2100	Historical baseline	1981-2000	2050	2081-2100
CMIP5	**ACCESS 1.0**	23.4	21.1	19.4	**18.2 (-13.7%)**	-19.3	-18.4	-17.6	-17.1 (7.0%)
	CanESM2	23.4	17.5	17.5	17.6 (0.5%)	-19.3	-16.2	-17.4	**-18.2 (-12.3%)**
	CSIRO Mk3.6.0	23.4	21.3	21.8	22.2 (3.5%)	-19.3	-21.2	-19.5	**-18.4 (12.9%)**
	IPSL CM5A-LR	23.4	19.5	20.2	**20.7 (6.4%)**	-19.3	-23.0	-24.8	-25.9 (-12/6%)
	Nor ESM1	23.4	14.9	14.9	14.8 (--0.4%)	-19.3	-16.2	-16.1	-16.0 (1.0%)
CMIP3	**CSIRO Mk3.5**	23.4	21.1	20.9	20.7 (-2.1)	-19.3	-19.3	-19.2	-19.1 (1.0%)
	ECHAM5	23.4	20.2	20.3	20.4 (0.8%)	-19.3	-19.3	-20.3	**-20.9 (-8.4%)**
	GFDL CM2.0	23.4	20.9	22.0	**22.8 (9.0%)**	-19.3	-21.1	-21.5	-21.8 (-3.6%)
	GFDL CM2.1	23.4	20.7	21.1	21.3 (3.3%)	-19.3	-18.9	-21.4	**-23.0 (-21.5%)**
	HadCM3	23.4	20.1	20.3	20.4 (1.8%)	-19.3	-18.6	-20.3	**-21.4 (-15.4%)**
	MIROC 3.2	23.4	20.8	20.1	**19.6 (5.6%)**	-19.3	-19.1	-20.5	**-21.5 (-12.5%)**

Table 7: As for Table 3, but for mean maximum sustained wind speed (m/s).

		Northern Hemisphere				Southern Hemisphere			
	Model	Historical baseline	1981-2000	2050	2081-2100	Historical baseline	1981-2000	2050	2081-2100
CMIP5	**ACCESS 1.0**	42.0	41.1	37.9	**35.8 (-13.1%)**	37.0	38.0	36.4	**35.27 (-7.3%)**
CMIP5	**CanESM2**	42.0	41.2	42.7	**43.6 (5.7%)**	37.0	39.3	40.4	40.8 (3.7%)
CMIP5	**CSIRO Mk3.6.0**	42.0	41.1	41.4	41.7 (1.4%)	37.0	40.9	40.4	40.0 (-2.3%)
CMIP5	**IPSL CM5A-LR**	42.0	43.4	43.7	43.4 (1.3%)	37.0	38.8	40.8	42.1 (8.6%)
CMIP5	**Nor ESM1**	42.0	39.0	34.7	**31.9 (-18.1%)**	37.0	35.5	31.5	**28.9 (-18.5%)**
CMIP3	**CSIRO Mk3.5**	42.0	36.2	37.7	37.8 (4.3%)	37.0	31.5	32.5	33.1 (5.3%)
CMIP3	**ECHAM5**	42.0	40.0	41.0	41.7 (4.3%)	37.0	35.7	32.3	**30.0 (-15.8%)**
CMIP3	**GFDL CM2.0**	42.0	34.3	35.8	36.7 (7.0%)	37.0	29.8	28.8	28.15 (-5.7%)
CMIP3	**GFDL CM2.1**	42.0	35.4	33.7	32.6 (-7.9%)	37.0	27.5	26.6	26.0 (-5.7%)
CMIP3	**HadCM3**	42.0	39.8	40.0	40.2 (1.2%)	37.0	41.9	40.6	39.8 (-5.0%)
CMIP3	**MIROC 3.2**	42.0	42.5	40.7	**39.5 (-7.0%)**	37.0	43.4	43.0	42.7 (-1.5%)

Table 8: As for Table 3, but for mean minimum central pressure (hPa).

		Northern Hemisphere				Southern Hemisphere			
	Model	Historical baseline	1981-2000	2050	2081-2100	Historical baseline	1981-2000	2050	2081-2100
CMIP5	**ACCESS 1.0**	970.4	960.8	966.0	**969.5 (0.9%)**	976.4	968.6	971.0	972.6 (0.4%)
	CanESM2	970.4	965.6	963.2	**961.5 (-0.4%)**	976.4	969.1	966.1	**964.1 (-0.5%)**
	CSIRO Mk3.6.0	970.4	961.5	960.2	959.4 (-0.2%)	976.4	962.8	964.0	964.8 (0.2%)
	IPSL CM5A-LR	970.4	961.4	960.4	959.7 (-0.2%)	976.4	970.4	967.2	965.1 (-0.5%)
	Nor ESM1	970.4	966.9	973.9	**978.5 (1.2%)**	976.4	971.7	977.2	**980.9 (-0.9%)**
CMIP3	**CSIRO Mk3.5**	970.4	970.4	968.6	967.4 (-0.3%)	976.4	980.9	979.5	978.5 (-0.2%)
	ECHAM5	970.4	966.4	965.5	964.9 (-0.1%)	976.4	975.0	979.1	981.8 (0.7%)
	GFDL CM2.0	970.4	974.2	970.6	**968.2 (-0.6%)**	976.4	983.4	985.3	986.5 (0.3%)
	GFDL CM2.1	970.4	972.9	974.9	976.2 (0.3%)	976.4	986.6	987.3	987.8 (0.1%)
	HadCM3	970.4	967.5	966.6	965.9 (-0.2%)	976.4	966.9	967.4	967.8 (0.1%)
	MIROC 3.2	970.4	962.7	966.7	**969.3 (0.7%)**	976.4	962.9	961.7	960.9 (-0.2%)

Ensemble results

It is of interest to examine the results of the analysis aggregated by model generation – that is the CMIP3 and CMIP5 model generations. The key difference between the two (aside from improvements in model parameterisations and resolution) is that the CMIP3 models were subjected to a dynamical downscaling process (Figure 2). This process has significant impacts on the resulting changes in the parameters. This is highlighted by the robust changes seen in all parameters for the CMIP3 ensemble.

Table 9: Ensemble mean peril matrix based on CMIP 3 and CMIP5 models. Bold values in the 2081-2100 column indicate where the majority of members have the same sign and are in the same direction as the mean, indicating a more likely outcome.

		Northern hemisphere				Southern hemisphere			
Parameter		Historical Baseline	1981-2000	2050	2081-2100	Historical Baseline	1981-2000	2050	2081-2100
Annual frequency (TCs/year)	CMIP5	24.7	24.7	27.3	**29.1**	13.2	13.2	13.6	13.4
	CMIP3	24.7	24.7	22.2	**20.5**	13.2	13.2	8.0	**4.6**
Genesis Latitude (degrees north)	CMIP5	13.2	14.0	13.6	**13.4**	-14.3	-13.8	-13.4	**-13.2**
	CMIP3	13.2	15.8	15.9	**15.9**	-14.3	-18.4	-19.5	**-20.3**
Mean latitude of peak intensity (degrees north)	CMIP5	23.4	18.9	18.7	18.7	-19.3	-19.0	-19.1	-19.1
	CMIP3	23.4	20.6	20.8	**20.9**	-19.3	-19.4	-20.5	**-21.3**
Mean maximum sustained wind speed (m/s)	CMIP5	42.0	41.2	40.1	39.4	37.0	38.5	37.9	**37.4**
	CMIP3	42.0	38.0	38.1	**38.1**	37.0	35.0	34.0	**33.3**
Mean minimum central pressure (hPa)	CMIP5	970.4	963.2	964.7	965.7	976.4	968.5	969.1	**969.5**
	CMIP3	970.4	969.0	968.8	**968.7**	976.4	975.9	976.7	**977.2**

Changes in the genesis latitude across the CMIP5 ensemble indicate an equatorward shift in TC genesis, which would increase the threat of TC impacts to those nations close to the equator (e.g. Nauru and Kiribati) compared with the historical records. The CMIP5 ensemble also shows no significant change to the latitude of peak intensity of TCs in either hemisphere. Only in the southern hemisphere is there a large change in the latitude of formation and peak intensity in the CMIP3 ensemble – for both parameters the change is in the order of 2° poleward.

Across both ensembles and both hemispheres, mean TC maximum intensity (measured both by minimum central pressure and maximum sustained winds) is projected to decline.

Ensemble mean changes in the relative proportions of different TC categories are presented in Figure 10. Note it is likely that the proportions of lower intensity storms could be influenced by the choice of quantile scaling applied to the TCLVs, but this is ignored due to the low impacts associated with tropical depressions and tropical storms compared to intense TCs (category 3-5). As such, the discussion focusses on the changes to the proportions of these intense events.

In both the northern and southern hemispheres, there is a weak increasing trend in the proportion of category 5 events. For the CMIP3 models, both the northern and southern hemispheres indicate a slight increase in the proportion of category 1 and 2 TCs, and no change or slight decline in the proportion of intense TCs (category 3-5).

The CMIP5 ensemble indicates an increase in the proportion of tropical storms, balanced by a decline in the proportion of category 1 TCs. There is an increase in the proportion of category 5 TCs in both hemispheres, balanced by declines in category 3 and/or category 4 TCs. These CMIP5 results are consistent with those reported by other researchers (e.g. Holland and Bruyère, 2013) – a flattening of the relative distribution of TC intensity. Distributions for each individual model are presented in the Appendix – Table 13 – Table 34.

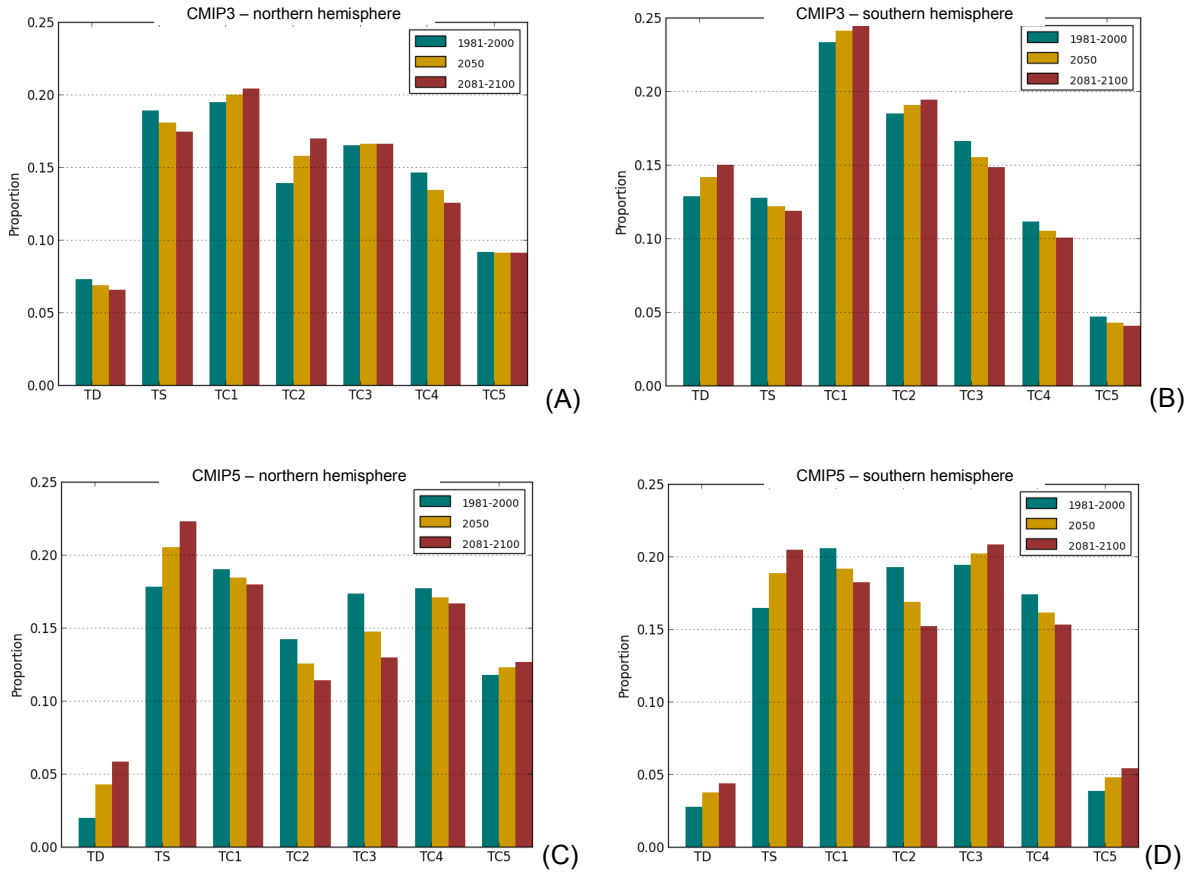

Figure 10: Relative proportion of TC intensity – multi model ensemble for (A) CMIP3 models in the northern hemisphere and (B) southern hemisphere, (C) CMIP5 models in the northern hemisphere and (D) southern hemisphere. Classification is based on central pressure, using the Saffir-Simpson Hurricane Intensity Scale (Table 1).

While the mean changes in the relative distributions are only moderate, some individual models display large changes in the proportion of TC intensities. In some cases, there are increases of over 100% within one category. The low numbers of events on which these relative distributions are based means that a small shift in the distribution can produce dramatic changes in the relative distribution. Part of this variability may be attributable to interannual variability in the simulated TCLV events, where the sampled time period for both the current and future climates represents only a small part of the true distribution of the future climate (note that significance testing was not performed on these relative distributions).

The analysis here indicates that the CMIP3 models project a modest decrease in the proportion of category 5 TCs in the southern hemisphere and little change in the northern hemisphere. The CMIP5 ensemble projects the proportion of category 5 TCs to be 39% higher by 2081-2100 in the southern hemisphere domain, but only 7% greater in the northern hemisphere.

While these results indicate a greater likelihood of occurrence of intense TCs, the actual number of intense TCs is also strongly dependent on the mean frequency of TCs. Of greatest significance is the combination of an increase in the proportion of intense TCs and marginal increase in mean frequency indicated by the CMIP5 ensemble for the southern hemisphere. Further increasing the threat of impacts is the ensemble trend for the formation region of TCs to shift closer to the equator. Such an outcome could result in increases in the impacts of TCs on nations in this region (Palau, Federated States of Micronesia and Republic of the Marshall Islands).

Table 10: Southern hemisphere ensemble relative distribution of intensity. Bold values indicate where the majority of members have the same sign and are in the same direction as the mean, indicating a more likely outcome.

	CMIP5			CMIP3			Baseline
Category	1981-2000	2050	2081-2100	1981-2000	2050	2081-2100	1981-2011
TC5	0.039	0.048 (23.6%)	**0.054 (39.0%)**	0.047	0.043 (-8.5%)	**0.041 (-13.8%)**	0.025
TC4	0.174	0.162 (-7.1%)	**0.153 (-11.9%)**	0.112	0.105 (-5.7%)	0.101 (-9.7%)	0.085
TC3	0.194	0.203 (4.2%)	0.209 (7.3%)	0.166	0.156 (-6.4%)	**0.149 (-10.7%)**	0.128
TC2	0.193	0.169 (-12.6%)	**0.153 (-21.0%)**	0.185	0.191 (3.1%)	0.195 (5.0%)	0.172
TC1	0.206	0.192 (-6.8%)	**0.183 (-11.4%)**	0.234	0.241 (3.3%)	0.246 (5.5%)	0.403
TS	0.165	0.189 (14.5%)	**0.205 (24.4%)**	0.128	0.122 (-4.2%)	0.119 (-6.9%)	0.145
TD	0.028	0.038 (34.3%)	**0.044 (56.4%)**	0.129	0.142 (10.2%)	**0.151 (17.0%)**	0.043

Table 11: Northern hemisphere ensemble relative distribution of intensity. Bold values indicate where the majority of members have the same sign and are in the same direction as the mean, indicating a more likely outcome.

	CMIP5			CMIP3			Baseline
Category	1981-2000	2050	2081-2100	1981-2000	2050	2081-2100	1981-2011
TC5	0.118	0.123 (4.2%)	**0.127 (7.3%)**	0.092	0.092 (-0.2%)	**0.092 (-0.4%)**	0.074
TC4	0.178	0.171 (-3.7%)	**0.167 (-6.0%)**	0.147	0.135 (-8.2%)	**0.126 (-14.0%)**	0.142
TC3	0.174	0.147 (-15.1%)	**0.130 (-25.2%)**	0.165	0.166 (0.7%)	0.167 (0.9%)	0.151
TC2	0.142	0.126 (-11.8%)	**0.114 (-19.7%)**	0.139	0.158 (13.3%)	**0.170 (22.1%)**	0.138
TC1	0.191	0.184 (-3.3%)	**0.180 (-5.5%)**	0.195	0.200 (2.8%)	**0.204 (4.8%)**	0.253
TS	0.178	0.205 (15.1%)	**0.223 (25.2%)**	0.189	0.181 (-4.5%)	**0.175 (-7.6%)**	0.154
TD	0.020	0.043 (116.0%)	**0.059 (194.0%)**	0.073	0.069 (-5.9%)	**0.066 (-9.8%)**	0.089

Summary

This project has examined changes in key parameters associated with TC activity in the Pacific region, with a view to informing risk modelling of current and future climate scenarios. By examining a number of sources of climate-conditioned TC information, changes in parameters describing TC activity in the current and future climate have been quantified. The range of projected changes, especially those derived from the latest generation of GCMs, generally provide only moderate confidence in the mean changes.

The CMIP3 models all indicate major decreases in TC annual frequency, especially for the southern hemisphere where the decrease ranges between -55% and -78%. Changes in the northern hemisphere are less consistent, ranging from +6.5% to -33%. The CMIP5 simulations indicate a wider range of changes: in the southern hemisphere frequency ranges from a decline of -25% to a doubling of frequency. The northern hemisphere ranges between declines of 16%, to an increase of over 60%, with the mean change an increase of 18%.

There is little change in mean maximum intensity across the ensemble. The majority of CMIP3 models indicate slight decline (on the order of 5%) in the southern hemisphere, but this change is not statistically significant. There is a slight increase in the northern hemisphere, but again it is not statistically significant. The CMIP5 models display a similar spread of results to the CMIP3 models. Of more significance are the changes in the proportion of intense TCs (category 5), especially for the CMIP5 ensemble where a robust increase is projected in the southern hemisphere.

The majority of CMIP5 indicate an equatorward shift in genesis latitude in both hemispheres. The CMIP3 models indicate a slight equatorward shift in the northern hemisphere and a poleward shift in the southern hemisphere of nearly 2°.

In terms of the latitude of peak intensity, the CMIP5 models are spread evenly with both equatorward and poleward changes indicated in both hemispheres. There is a strong signal of a poleward shift across the CMIP3 models for the southern hemisphere, with an average shift of 2° indicated amongst these models.

A key difference between the CMIP3 and CMIP5 simulations is the dynamical downscaling performed on the CMIP3 simulations. For these models, the forcing process (bias-corrected sea surface temperatures) has resulted in a consistent signal in the changes for many of the parameters especially in the southern hemisphere domain. This may in fact be masking the true nature of the changes to the climate system as simulated by the parent GCM.

The results from the CMIP5 models (for which no dynamical downscaling was required) indicate that the CMIP5 models generally have better skill in replicating the behaviour of TCs in the current climate for the southern hemisphere, especially in terms of annual frequency and genesis latitude. As such, more confidence can be placed on the latest generation of models without relying on intermediate processes such as downscaling. However, there may still be additional skill gained by downscaling TCLVs using regional-scale models, especially in terms of projected changes in TC intensity.

The effects of the analysed changes in TC behaviour on the frequency and intensity of TCs impacting individual nations in the Pacific cannot be directly quantified from these results alone. A more thorough examination of the hazard posed by TCs will bear this out, and is being completed as part of the PACCSAP Science Program in collaboration with CSIRO.

Appendix

Climate modelling groups

Table 12: Modelling groups performing general circulation model simulations as part of the CMIP3 and CMIP5 programs, and Model Name used in this project.

Modelling centre	Institute ID	Mode Name
Commonwealth Scientific and Industrial Research Organization (CSIRO) and Bureau of Meteorology (BoM), Australia	CSIRO-BOM	ACCESS1.0
Canadian Centre for Climate Modelling and Analysis	CCCMA	CanESM2
Commonwealth Scientific and Industrial Research Organization in collaboration with Queensland Climate Change Centre of Excellence	CSIRO-QCCCE	CSIRO-Mk3.6.0
Institut Pierre-Simon Laplace	IPSL	IPSL-CM5A-LR
Norwegian Climate Centre	NCC	NorESM1-M
Commonwealth Scientific and Industrial Research Organization Atmospheric Research	CSIRO	CSIRO-Mk3.5
Hadley Centre for Climate Prediction and Research / Met Office	UKMO	UKMO-HadCM3
Max Planck Institute for Meteorology	MPI	ECHAM5/MPI-OM
US Dept. of Commerce / NOAA / Geophysical Fluid Dynamics Laboratory	GFDL	GFDL-CM2.0 GFDL-CM2.1
Center for Climate System Research (The University of Tokyo), National Institute for Environmental Studies, and Frontier Research Center for Global Change (JAMSTEC)	JAMSTEC	MIROC3.2 (medres)

Relative distribution of TC intensity

These tables present the relative distribution of intensity for current and future climate simulations. Also included are the current baseline relative distributions for reference. Categorisations are based on the minimum central pressure, using the Saffir-Simpson Hurricane Intensity Scale.

Southern hemisphere domain

Table 13: ACCESS 1.0 southern hemisphere relative distribution of intensity.

Category	1981-2000	2050	2081-2100	Baseline
TC5	0.07	0.055 (-21.5%)	0.045 (-35.8%)	0.025
TC4	0.112	0.114 (+1.3%)	0.115 (+2.2%)	0.085
TC3	0.225	0.232 (+3.5%)	0.238 (+5.9%)	0.128
TC2	0.207	0.176 (-14.9%)	0.156 (-24.8%)	0.172
TC1	0.165	0.169 (+2.6%)	0.172 (+4.4%)	0.403
TS	0.168	0.183 (+8.6%)	0.193 (+14.4%)	0.145
TD	0.053	0.07 (+33.4%)	0.082 (+55.7%)	0.043

Table 14: CanESM 2 southern hemisphere relative distribution of intensity.

Category	1981-2000	2050	2081-2100	Baseline
TC5	0.056	0.105 (+89.6%)	0.139 (+149.4%)	0.025
TC4	0.142	0.136 (-4.1%)	0.133 (-6.9%)	0.085
TC3	0.181	0.164 (-9.0%)	0.154 (-14.9%)	0.128
TC2	0.215	0.162 (-24.7%)	0.127 (-41.2%)	0.172
TC1	0.194	0.219 (+12.5%)	0.235 (+20.8%)	0.403
TS	0.177	0.19 (+7.4%)	0.199 (+12.3%)	0.145
TD	0.035	0.023 (-34.0%)	0.015 (-56.6%)	0.043

Table 15: CSIRO Mk 3.6.0 southern hemisphere relative distribution of intensity.

Category	1981-2000	2050	2081-2100	Baseline
TC5	0.03	0.031 (+3.6%)	0.031 (+6.0%)	0.025
TC4	0.266	0.255 (-4.5%)	0.247 (-7.4%)	0.085
TC3	0.24	0.233 (-2.9%)	0.229 (-4.8%)	0.128
TC2	0.151	0.152 (+0.5%)	0.152 (+0.8%)	0.172
TC1	0.158	0.147 (-7.2%)	0.139 (-12.0%)	0.403
TS	0.141	0.172 (+21.8%)	0.193 (+36.3%)	0.145
TD	0.013	0.011 (-19.1%)	0.009 (-31.8%)	0.043

Table 16: IPSL CM5A LR southern hemisphere relative distribution of intensity.

Category	1981-2000	2050	2081-2100	Baseline
TC5	0.014	0.027 (+95.3%)	0.035 (+158.9%)	0.025
TC4	0.151	0.158 (+5.0%)	0.163 (+8.3%)	0.085
TC3	0.151	0.218 (+44.5%)	0.262 (+74.1%)	0.128
TC2	0.247	0.248 (+0.4%)	0.248 (+0.7%)	0.172
TC1	0.342	0.256 (-25.2%)	0.199 (-42.0%)	0.403
TS	0.096	0.094 (-2.3%)	0.092 (-3.9%)	0.145
TD	0	0 (0.0%)	0 (0.0%)	0.043

Table 17: NorESM 1M southern hemisphere relative distribution of intensity.

Category	1981-2000	2050	2081-2100	Baseline
TC5	0.025	0.023 (-9.6%)	0.021 (-16.0%)	0.025
TC4	0.2	0.146 (-27.2%)	0.109 (-45.4%)	0.085
TC3	0.175	0.166 (-5.3%)	0.16 (-8.8%)	0.128
TC2	0.146	0.106 (-27.3%)	0.08 (-45.5%)	0.172
TC1	0.171	0.169 (-1.2%)	0.168 (-2.0%)	0.403
TS	0.243	0.306 (+26.2%)	0.349 (+43.6%)	0.145
TD	0.039	0.084 (+113.3%)	0.113 (+188.8%)	0.043

Table 18: CSIRO Mk 3.5 southern hemisphere relative distribution of intensity.

Category	1981-2000	2050	2081-2100	Baseline
TC5	0.025	0.017 (-31.0%)	0.012 (-51.7%)	0.025
TC4	0.108	0.129 (+19.1%)	0.143 (+31.8%)	0.085
TC3	0.148	0.123 (-16.5%)	0.107 (-27.5%)	0.128
TC2	0.167	0.174 (+4.0%)	0.179 (+6.6%)	0.172
TC1	0.256	0.238 (-7.0%)	0.226 (-11.7%)	0.403
TS	0.143	0.193 (+35.0%)	0.226 (+58.3%)	0.145
TD	0.153	0.125 (-17.9%)	0.107 (-29.8%)	0.043

Table 19: ECHAM5 southern hemisphere relative distribution of intensity.

Category	1981-2000	2050	2081-2100	Baseline
TC5	0.05	0.031 (-36.8%)	0.019 (-61.4%)	0.025
TC4	0.12	0.1 (-16.6%)	0.087 (-27.6%)	0.085
TC3	0.179	0.153 (-15.0%)	0.135 (-25.0%)	0.128
TC2	0.209	0.188 (-10.4%)	0.173 (-17.3%)	0.172
TC1	0.179	0.262 (+46.1%)	0.317 (+76.9%)	0.403
TS	0.113	0.091 (-19.1%)	0.077 (-31.9%)	0.145
TD	0.15	0.175 (+17.2%)	0.192 (+28.6%)	0.043

Table 20: GFDL CM2.0 southern hemisphere relative distribution of intensity.

Category	1981-2000	2050	2081-2100	Baseline
TC5	0.027	0.011 (-60.0%)	0 (-100.0%)	0.025
TC4	0.09	0.036 (-60.0%)	0 (-100.0%)	0.085
TC3	0.149	0.184 (+23.9%)	0.208 (+39.8%)	0.128
TC2	0.158	0.172 (+9.2%)	0.182 (+15.3%)	0.172
TC1	0.212	0.256 (+21.0%)	0.286 (+35.0%)	0.403
TS	0.135	0.14 (+3.4%)	0.143 (+5.7%)	0.145
TD	0.23	0.201 (-12.5%)	0.182 (-20.9%)	0.043

Table 21: GFDL CM2.1 southern hemisphere relative distribution of intensity.

Category	1981-2000	2050	2081-2100	Baseline
TC5	0.026	0.024 (-6.2%)	0.023 (-10.3%)	0.025
TC4	0.068	0.083 (+20.7%)	0.092 (+34.5%)	0.085
TC3	0.132	0.143 (+7.7%)	0.149 (+12.8%)	0.128
TC2	0.137	0.124 (-9.6%)	0.115 (-15.9%)	0.172
TC1	0.197	0.196 (-0.4%)	0.195 (-0.6%)	0.403
TS	0.201	0.136 (-32.5%)	0.092 (-54.2%)	0.145
TD	0.239	0.296 (+23.6%)	0.333 (+39.3%)	0.043

Table 22: HadCM3 southern hemisphere relative distribution of intensity.

Category	1981-2000	2050	2081-2100	Baseline
TC5	0.03	0.049 (+60.7%)	0.061 (+101.2%)	0.025
TC4	0.152	0.134 (-11.7%)	0.122 (-19.5%)	0.085
TC3	0.237	0.212 (-10.7%)	0.195 (-17.8%)	0.128
TC2	0.232	0.21 (-9.6%)	0.195 (-16.0%)	0.172
TC1	0.258	0.279 (+8.2%)	0.293 (+13.6%)	0.403
TS	0.091	0.102 (+12.4%)	0.11 (+20.7%)	0.145
TD	0	0.015 (0.0%)	0.024 (0.0%)	0.043

Table 23: MIROC 3.2 southern hemisphere relative distribution of intensity.

Category	1981-2000	2050	2081-2100	Baseline
TC5	0.125	0.127 (+1.9%)	0.129 (+3.2%)	0.025
TC4	0.132	0.15 (+13.3%)	0.161 (+22.2%)	0.085
TC3	0.153	0.119 (-22.0%)	0.097 (-36.7%)	0.128
TC2	0.208	0.277 (+32.9%)	0.323 (+54.8%)	0.172
TC1	0.299	0.216 (-27.6%)	0.161 (-46.0%)	0.403
TS	0.083	0.072 (-13.5%)	0.065 (-22.6%)	0.145
TD	0	0.039 (0.0%)	0.065 (0.0%)	0.043

Northern hemisphere domain

Table 24: ACCESS 1.0 northern hemisphere relative distribution of intensity.

Category	1981-2000	2050	2081-2100	Baseline
TC5	0.155	0.127 (-18.2%)	0.108 (-30.4%)	0.074
TC4	0.152	0.125 (-17.2%)	0.108 (-28.6%)	0.142
TC3	0.205	0.15 (-26.8%)	0.113 (-44.7%)	0.151
TC2	0.106	0.132 (+24.8%)	0.15 (+41.3%)	0.138
TC1	0.148	0.167 (+12.8%)	0.179 (+21.4%)	0.253
TS	0.208	0.234 (+12.2%)	0.251 (+20.3%)	0.154
TD	0.027	0.065 (+145.7%)	0.091 (+242.9%)	0.089

Table 25: CanESM 2 northern hemisphere relative distribution of intensity.

Category	1981-2000	2050	2081-2100	Baseline
TC5	0.08	0.112 (+40.8%)	0.134 (+67.9%)	0.074
TC4	0.168	0.178 (+6.3%)	0.185 (+10.5%)	0.142
TC3	0.191	0.18 (-6.0%)	0.172 (-9.9%)	0.151
TC2	0.174	0.143 (-17.7%)	0.123 (-29.5%)	0.138
TC1	0.23	0.214 (-7.2%)	0.203 (-12.0%)	0.253
TS	0.142	0.154 (+8.3%)	0.162 (+13.9%)	0.154
TD	0.015	0.019 (+25.9%)	0.022 (+43.2%)	0.089

Table 26: CSIRO Mk 3.6.0 northern hemisphere relative distribution of intensity.

Category	1981-2000	2050	2081-2100	Baseline
TC5	0.122	0.147 (+20.7%)	0.164 (+34.6%)	0.074
TC4	0.179	0.197 (+10.3%)	0.21 (+17.2%)	0.142
TC3	0.181	0.154 (-14.7%)	0.136 (-24.5%)	0.151
TC2	0.172	0.127 (-26.1%)	0.097 (-43.5%)	0.138
TC1	0.2	0.182 (-8.8%)	0.17 (-14.7%)	0.253
TS	0.134	0.174 (+30.2%)	0.201 (+50.4%)	0.154
TD	0.014	0.019 (+35.7%)	0.022 (+59.5%)	0.089

Table 27: IPSL CM5A LR northern hemisphere relative distribution of intensity.

Category	1981-2000	2050	2081-2100	Baseline
TC5	0.126	0.145 (+15.3%)	0.158 (+25.5%)	0.074
TC4	0.217	0.213 (-1.9%)	0.21 (-3.2%)	0.142
TC3	0.143	0.138 (-3.6%)	0.135 (-6.0%)	0.151
TC2	0.133	0.136 (+2.0%)	0.137 (+3.3%)	0.138
TC1	0.203	0.181 (-10.9%)	0.166 (-18.2%)	0.253
TS	0.161	0.168 (+4.8%)	0.174 (+7.9%)	0.154
TD	0.017	0.019 (+11.1%)	0.021 (+18.5%)	0.089

Table 28: NorESM 1M northern hemisphere relative distribution of intensity.

Category	1981-2000	2050	2081-2100	Baseline
TC5	0.107	0.084 (-21.1%)	0.069 (-35.1%)	0.074
TC4	0.172	0.142 (-17.4%)	0.122 (-29.0%)	0.142
TC3	0.148	0.115 (-22.0%)	0.093 (-36.7%)	0.151
TC2	0.127	0.09 (-29.3%)	0.065 (-48.8%)	0.138
TC1	0.172	0.178 (+3.9%)	0.183 (+6.5%)	0.253
TS	0.247	0.297 (+19.8%)	0.329 (+33.1%)	0.154
TD	0.027	0.094 (+241.6%)	0.138 (+402.7%)	0.089

Table 29: CSIRO Mk 3.5 northern hemisphere relative distribution of intensity.

Category	1981-2000	2050	2081-2100	Baseline
TC5	0.096	0.13 (+35.2%)	0.152 (+58.6%)	0.074
TC4	0.144	0.133 (-7.9%)	0.125 (-13.2%)	0.142
TC3	0.155	0.128 (-17.8%)	0.109 (-29.6%)	0.151
TC2	0.099	0.115 (+15.9%)	0.125 (+26.4%)	0.138
TC1	0.195	0.176 (-9.5%)	0.164 (-15.8%)	0.253
TS	0.189	0.216 (+14.3%)	0.234 (+23.8%)	0.154
TD	0.121	0.102 (-15.6%)	0.09 (-26.0%)	0.089

Table 30: ECHAM5 northern hemisphere relative distribution of intensity.

Category	1981-2000	2050	2081-2100	Baseline
TC5	0.091	0.095 (+4.2%)	0.098 (+6.9%)	0.074
TC4	0.172	0.137 (-20.4%)	0.113 (-34.0%)	0.142
TC3	0.168	0.197 (+17.4%)	0.216 (+29.0%)	0.151
TC2	0.161	0.191 (+18.5%)	0.211 (+30.8%)	0.138
TC1	0.195	0.205 (+4.8%)	0.211 (+8.1%)	0.253
TS	0.149	0.132 (-11.0%)	0.121 (-18.3%)	0.154
TD	0.064	0.043 (-32.7%)	0.029 (-54.4%)	0.089

Table 31: GFDL CM2.0 northern hemisphere relative distribution of intensity.

Category	1981-2000	2050	2081-2100	Baseline
TC5	0.086	0.085 (-1.0%)	0.085 (-1.7%)	0.074
TC4	0.11	0.142 (+29.2%)	0.163 (+48.7%)	0.142
TC3	0.148	0.156 (+4.8%)	0.16 (+8.1%)	0.151
TC2	0.119	0.128 (+7.8%)	0.134 (+13.0%)	0.138
TC1	0.175	0.187 (+6.9%)	0.195 (+11.6%)	0.253
TS	0.255	0.218 (-14.8%)	0.192 (-24.6%)	0.154
TD	0.107	0.085 (-20.7%)	0.07 (-34.5%)	0.089

Table 32: GFDL CM2.1 northern hemisphere relative distribution of intensity.

Category	1981-2000	2050	2081-2100	Baseline
TC5	0.068	0.065 (-4.9%)	0.062 (-8.1%)	0.074
TC4	0.126	0.108 (-14.5%)	0.096 (-24.1%)	0.142
TC3	0.159	0.138 (-12.7%)	0.125 (-21.2%)	0.151
TC2	0.126	0.147 (+17.1%)	0.162 (+28.4%)	0.138
TC1	0.217	0.206 (-5.0%)	0.199 (-8.4%)	0.253
TS	0.229	0.233 (+1.6%)	0.235 (+2.7%)	0.154
TD	0.076	0.103 (+36.3%)	0.121 (+60.6%)	0.089

Table 33: HadCM3 northern hemisphere relative distribution of intensity.

Category	1981-2000	2050	2081-2100	Baseline
TC5	0.069	0.077 (+12.4%)	0.083 (+20.7%)	0.074
TC4	0.163	0.154 (-5.6%)	0.147 (-9.4%)	0.142
TC3	0.194	0.193 (-0.7%)	0.192 (-1.1%)	0.151
TC2	0.169	0.184 (+9.0%)	0.194 (+15.0%)	0.138
TC1	0.196	0.209 (+6.8%)	0.218 (+11.3%)	0.253
TS	0.165	0.137 (-16.6%)	0.119 (-27.6%)	0.154
TD	0.045	0.046 (+1.8%)	0.046 (+3.0%)	0.089

Table 34: MIROC 3.2 northern hemisphere relative distribution of intensity.

Category	1981-2000	2050	2081-2100	Baseline
TC5	0.141	0.098 (-30.5%)	0.069 (-50.8%)	0.074
TC4	0.164	0.133 (-19.1%)	0.112 (-31.8%)	0.142
TC3	0.167	0.186 (+11.1%)	0.198 (+18.5%)	0.151
TC2	0.162	0.182 (+12.2%)	0.195 (+20.3%)	0.138
TC1	0.191	0.219 (+14.8%)	0.238 (+24.7%)	0.253
TS	0.149	0.149 (-0.1%)	0.149 (-0.2%)	0.154
TD	0.026	0.034 (+31.0%)	0.04 (+51.7%)	0.089

References

Abbs, D., 2012: The impact of climate change on the climatology of tropical cyclones in the Australian region. *CSIRO Climate Adaptation Flagship working paper series*, CSIRO, pp 16.

Abbs, D. J., S. Aryal, E. Campbell, J. McGregor, K. Nguyen, M. Palmer, T. Rafter, I. Watterson, and B. Bates, 2006: *Projections of Extreme Rainfall and Cyclones: Final Report to the Australian Greenhouse Office*, CSIRO Marine and Atmospheric Research, Aspendale, Report Nº.:C/0971.

Brunt, A. T., 1969: Low latitude cyclones. *Australian Meteorological Magazine*, **17**, 67–90

Bureau of Meteorology and CSIRO, 2011: Climate Change in the Pacific: Scientific Assessment and New Research: Volume 1: Regional Overview, CSIRO: available online at http://www.pacificclimatechangescience.org/

Harper, B. A., 2002: Tropical Cyclone Parameter Estimation in the Australian Region: Wind Pressure Relationships and Related Issues for Engineering Planning and Design.

Harper, B. A., J. D. Kepert, and J. D. Ginger, 2010: Guidelines for converting between various wind averaging periods in tropical cyclone conditions. WMO/TD-Nº.1555.

Hemer, M. A., K. L. McInnes, and R. Ranasinghe, 2012: Climate and variability bias adjustment of climate model-derived winds for a southeast Australian dynamical wave model. *Ocean Dynamics*, **62,** 87-104.

Holland, G., 2008: A Revised Hurricane Pressure-Wind Model. *Monthly Weather Review*, **136,** 3432-3445.

Holland, G. J., and C. L. Bruyère, 2013: Recent intense hurricane response to global climate change. *Climate Dynamics***,** 11-11.

Katzfey, J., J. McGregor, K. Nguyen, and M. Thatcher, 2009: Dynamical downscaling techniques: Impacts on regional climate change signals. *MODSIM09 Int. Congress on Modelling and Simulation. www.mssanz.org.au/modsim09 I*, 2377-2383.

Knapp, K. R., M. C. Kruk, D. H. Levinson, H. J. Diamond, and C. J. Neumann, 2010: The International Best Track Archive for Climate Stewardship (IBTrACS): Unifying tropical cyclone best track data. *Bulletin of the American Meteorological Society*, **91,** 363-376.

McGregor, J., M. R. Dix, K. Hamilton, and W. Ohfuchi, 2008: An Updated Description of the Conformal-Cubic Atmospheric Model. *High Resolution Numerical Modelling of the Atmosphere and Ocean*, Springer, 51-75.

Meehl, G. A., and Coauthors, 2012: Relative outcomes of climate change mitigation related to global temperature versus sea-level rise. *Nature Climate Change*, **2,** 576-580.

Meehl, G. A., and Coauthors, 2007: Global Climate Projections. *Climate Change 2007: The Physical Science Basis. Contribution of Working Group I to the Fourth Assessment Report of the Intergovernmental Panel on Climate Change*, Cambridge University Press, 747-846.

Nakicenovic, N., and R. Swart, 2000: *Special Report on Emissions Scenarios.* Cambridge University Press.

Nguyen, K. C., and K.J.E. Walsh, 2001: Interannual, decadal, and transient greenhouse simulation of tropical cyclone-like vortices in a regional climate model of the South Pacific. *Journal of Climate*, **14**, 3043-3054

van Vuuren, D. P., and Coauthors, 2011: The representative concentration pathways: an overview. *Climatic Change*, **109,** 5-13.

Walsh, K. J. E., and J.I. Syktus, 2003: Simulations of observed interannual variability of tropical cyclone formation east of Australia. *Atmospheric Science Letters*, **4** (1-4), 28-40.